JOURNAL OF COMPUTATIONAL PHYSICS 28, 14–42 (1978)

Kármán Vortex Street behind a Circular Cylinder by the Series Truncation Method

V. A. PATEL

Department of Mathematics, Humboldt State University, Arcata, California 95521

Received April 12, 1977; revised July 20, 1977

Semianalytical solutions of the Navier-Stokes equations are presented for two-dimensional, viscous, and incompressible flow past a circular cylinder for Reynolds numbers 100, 200 and 500. The stream and vorticity functions are expanded in a finite Fourier series and then substituted in the Navier-Stokes equations. This leads to a system of coupled parabolic partial differential equations which are solved numerically. In order to excite the flow an asymmetric disturbance in the form of rotation at a constant angular velocity of a cylinder in clockwise and counterclockwise directions is introduced for a short time. This small disturbance very slowly triggers the start of vortex shedding. The flow pattern in the separated region, lift and separation angle oscillate with a definite pattern. The calculated drag, lift, pressure and vorticity distributions around the surface, separation angle and Strouhal number are compared with similar calculations and with available experimental data. Also, a comparison of the calculations has been made for Reynolds number 100 with $N = 25$ and $N = 40$.

1. INTRODUCTION

The general features of the flow of a viscous fluid past a circular cylinder are known from experiments. At low Re ($= 2aU/\nu$, where a is the radius of the cylinder, U is the free stream velocity and ν is the kinematic viscocity) a steady symmetrical flow exists. The appearance of a wake first occurs at a Reynolds number Re of order 1, and the flow separates from the rear of the cylinder forming a recirculating eddy for Re greater than 6. On the other hand, it is shown by Homann [1], Kovaszny [2] and Taneda [3] that above Re = 40, the flow becomes unstable and periodic and transforms into the so-called Kármán Vortex street. Bénard [4] photographed and Von Kármán [5] proposed a theoretical model to predict the spacing ratio of the vortex street. Relf and Simmons [6] and Rosko [7] measured the shedding frequencies.

It is reasonable to use the Navier–Stokes equations to describe the motions of the viscous fluid in the case of Reynolds numbers which do not exceed certain limits. Since the Navier–Stokes equations are nonlinear, the exact solutions of the flow past bodies of finite size are still out of reach. Therefore, in order to discuss such flows, it is necessary to derive approximate solutions. These solutions may be either numerical solutions of the exact Navier–Stokes equations, or solutions—analytical or nume-

0021-9991/78/0281–0014$02.00/0

rical—of approximate equations. Although a large number of numerical calculations of the flow around a circular cylinder have been presented in the literature, there are not many without symmetry conditions. Jain and Rao [8] removed the symmetry condition and their computations do not show signs of the formation of Kármán Vortex street for Re = 100 up to $t = 52$. It seems natural to expect that above the critical Reynolds number the small disturbance, which is hidden in the uniform flow, gives rise to Kármán Vortex street. Fromm and Harlow [9] accomplished perturbation by artifically increasing the vorticity by a small amount at three mesh points just in front of the obstacle. Hirota and Miyakoda [10] have not added any disturbance purposely, still they were able to produce an asymmetrical configuration. This was indeed caused by truncation error, which originated from the procedure of scanning mesh in computation. The numerical solutions of Kármán Vortex street were obtained by Thoman and Szewczyk [11] by impulsively rotating the cylinder in one direction for a short time and by Jordan and Fromm [12] by impulsively twisting the cylinder counterclockwise, stopping, twisting clockwise and stopping, for a short time. Also Dawson and Marcus [13] and Jain and Goel [14] treated the unsteady asymmetric problem by the method of finite differences. Lin, Pepper and Lee [15] compared three finite-difference techniques and obtained numerical solutions of Kármán Vortex street around a circular cylinder for Re = 80 and 100.

Desai [16] obtained analytic solutions by expanding the stream and vorticity functions in finite Fourier series for steady flow of a viscous incompressible fluid past a circular cylinder for Re = 1 — 40. Underwood [17], Dennis and Shimshoni [18] and Nieuwstadt and Keller [19] obtained the semianalytic solutions for steady flows. Collins and Dennis [20] and Patel [21] obtained the semianalytic solutions for impulsively started symmetric flows. This study deals with the semianalytic solutions of the impulsively started unsteady flow past a circular cylinder of Kármán Vortex street for Re = 100, 200 and 500. The fluid is assumed to be homogeneous, incompressible, and governed by the Navier–Stokes equations.

2. Basic Equations and Analysis

Consider the unsteady laminar flow of a viscous incompressible flow past a circular cylinder of radius a when the flow starts at time $t = 0$ with a constant velocity U in the opposite direction $\theta = 0$ as shown in Fig. 1. The governing equation of motion in nondimensional form in polar coordinates can be written as [21]

$$\frac{\partial \zeta}{\partial t} + \frac{1}{r}\left(\frac{\partial \Psi}{\partial \theta}\frac{\partial \zeta}{\partial r} - \frac{\partial \Psi}{\partial r}\frac{\partial \zeta}{\partial \theta}\right) = \frac{2}{\mathrm{Re}}\nabla^2\zeta, \tag{2.1}$$

where

$$\nabla^2 = \frac{\partial^2}{\partial r^2} + \frac{1}{r}\frac{\partial}{\partial r} + \frac{1}{r^2}\frac{\partial^2}{\partial \theta^2}. \tag{2.2}$$

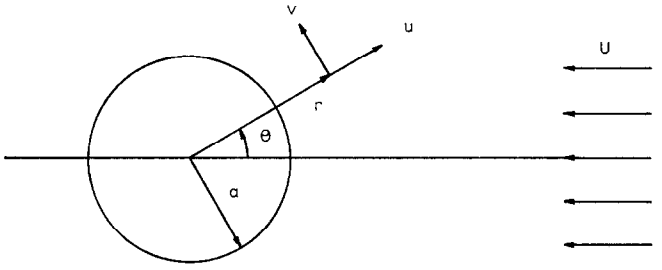

FIG. 1. Polar coordinate system.

The stream function Ψ, the vorticity ζ and the velocity components u and v in the r and θ directions are connected by the relations

$$\zeta = -\nabla^2\Psi, \tag{2.3}$$

$$u = \frac{1}{r}\frac{\partial\Psi}{\partial\theta}, \qquad v = -\frac{\partial\Psi}{\partial r}. \tag{2.4}$$

In order to excite the flow, an asymmetric disturbance in the form of a rotation of the cylinder at a constant velocity is to be introduced for a short time; therefore, we have at $r = 1$,

$$u = 0 \qquad \text{and} \qquad v = \omega.$$

As the distance from the cylinder becomes very large, it is assumed that the flow will approach more and more that of an ideal flow. These boundary conditions can be written as

For $t \geqslant 0$

$$\Psi = 0 \qquad \text{and} \qquad \partial\Psi/\partial r = -\omega \qquad \text{at} \quad r = 1$$

and (2.5)

$$\Psi = -(r - 1/r)\sin\theta \qquad \text{as} \quad r \to \infty.$$

The logarithmic transformation $\xi = \ln r$ of the radial coordinate is desirable since the cells of the log–polar grid are small near the cylinder where the largest gradients occur in the flow. Equations (2.1) and (2.2) reduce to

$$\frac{\partial\zeta}{\partial t} + e^{-2\xi}\left(\frac{\partial\Psi}{\partial\theta}\frac{\partial\zeta}{\partial\xi} - \frac{\partial\Psi}{\partial\xi}\frac{\partial\zeta}{\partial\theta}\right) = \frac{2}{\mathrm{Re}}\nabla^2\zeta, \tag{2.6}$$

where

$$\nabla^2 = e^{-2\xi}\left(\frac{\partial^2}{\partial\xi^2} + \frac{\partial^2}{\partial\theta^2}\right). \tag{2.7}$$

For convenience of numerical computation, let us write

$$\Psi = -\omega\xi + \psi. \tag{2.8}$$

Then Eqs. (2.6) and (2.7) further reduce to

$$\frac{\partial \zeta}{\partial t} + e^{-2\xi}\left(\frac{\partial \psi}{\partial \theta}\frac{\partial \zeta}{\partial \xi} - \frac{\partial \psi}{\partial \xi}\frac{\partial \zeta}{\partial \theta}\right) + \omega e^{-2\xi}\frac{\partial \zeta}{\partial \theta} = \frac{2}{\mathrm{Re}}\nabla^2\zeta, \tag{2.9}$$

where

$$\zeta = -\nabla^2\psi. \tag{2.10}$$

Let us assume ψ is a reasonably well-behaved function, throughout the domain $-\pi < \theta \leqslant \pi$, so it can be formally represented in a Fourier series

$$\psi(\xi, \theta, t) = f_0(\xi, t) + \sum_{n=1}^{\infty}\left(f_n(\xi, t)\sin n\theta + g_n(\xi, t)\cos n\theta\right), \tag{2.11}$$

where $f_0(\xi, t)$, $f_n(\xi, t)$ and $g_n(\xi, t)$ are the functions to be determined.

The substitution of (2.11) in (2.10) yields

$$\zeta(\xi, \theta, t) = -F_0(\xi, t) - \sum_{n=1}^{\infty}\left(F_n(\xi, t)\sin n\theta + G_n(\xi, t)\cos n\theta\right), \tag{2.12}$$

where

$$F_0(\xi, t) = e^{-2\xi}\left(\frac{\partial^2 f_0}{\partial \xi^2}\right), \qquad F_n(\xi, t) = e^{-2\xi}\left(\frac{\partial^2 f_n}{\partial \xi^2} - n^2 f_n\right),$$

and

$$G_n(\xi, t) = e^{-2\xi}\left(\frac{\partial^2 g_n}{\partial \xi^2} - n^2 g_n\right). \tag{2.13}$$

Substitution of (2.11) and (2.12) in (2.9) leads to an equation in which the terms in $\sin n\theta$ and $\cos n\theta$ are linearly independent, so the equation is satisfied only if the coefficients of $\sin n\theta$ and $\cos n\theta$ are identically equal to zero. This leads to

$$\frac{\partial F_0}{\partial t} + e^{-2\xi}\left[-\frac{2}{\mathrm{Re}}\frac{\partial^2 F_0}{\partial \xi^2} + \sum_{m=1}^{\infty}\frac{m}{2}\left(f_m\frac{\partial G_m}{\partial \xi} - g_m\frac{\partial F_m}{\partial \xi} - F_m\frac{\partial g_m}{\partial \xi} + G_m\frac{\partial f_m}{\partial \xi}\right)\right] = 0, \tag{2.14}$$

$$\begin{aligned}\frac{\partial F_n}{\partial t} + e^{-2\xi}\Bigg[&-\frac{2}{\mathrm{Re}}\left(\frac{\partial^2 F_n}{\partial \xi^2} - n^2 F_n\right) - n\omega G_n + n\left(G_n\frac{\partial f_0}{\partial \xi} - g_n\frac{\partial F_0}{\partial \xi}\right)\\ &+ \sum_{m=1}^{\infty}\frac{m}{2}\left\{f_m\left(\frac{\partial F_{m+n}}{\partial \xi} - \frac{\partial F_{m-n}}{\partial \xi}\right) + g_m\left(\frac{\partial G_{m+n}}{\partial \xi} - \frac{\partial G_{m-n}}{\partial \xi}\right)\right.\\ &\left.- F_m\left(\frac{\partial f_{m+n}}{\partial \xi} - \frac{\partial f_{m-n}}{\partial \xi}\right) - G_m\left(\frac{\partial g_{m+n}}{\partial \xi} - \frac{\partial g_{m-n}}{\partial \xi}\right)\right\}\Bigg] = 0\end{aligned}$$

$$\text{for} \quad n = 1, 2, \ldots, \tag{2.15}$$

and

$$\frac{\partial G_n}{\partial t} + e^{-2\xi}\left[-\frac{2}{\mathrm{Re}}\left(\frac{\partial^2 G_n}{\partial \xi^2} - n^2 G_n\right) + n\left(f_n \frac{\partial F_0}{\partial \xi} - F_n \frac{\partial f_0}{\partial \xi}\right) + n\omega F_n \right.$$
$$+ \sum_{m=1}^{\infty} \frac{m}{2}\left\{f_m\left(\frac{\partial G_{m+n}}{\partial \xi} + \frac{\partial G_{m-n}}{\partial \xi}\right) - g_m\left(\frac{\partial F_{m+n}}{\partial \xi} + \frac{\partial F_{m-n}}{\partial \xi}\right)\right.$$
$$\left.\left. - F_m\left(\frac{\partial g_{m+n}}{\partial \xi} + \frac{\partial g_{m-n}}{\partial \xi}\right) + G_m\left(\frac{\partial f_{m+n}}{\partial \xi} + \frac{\partial f_{m-n}}{\partial \xi}\right)\right\}\right] = 0$$
$$\text{for} \quad n = 1, 2,..., \quad (2.16)$$

where

$$F_{-n} = -F_n\,, \quad G_{-n} = G_n\,, \quad f_{-n} = -f_n \qquad \text{and} \qquad g_{-n} = g_n\,. \quad (2.17)$$

The subscript n represents the nth-order problem. The problem of each order is indeterminate, possessing infinitely more unknowns than equations. This difficulty can be circumvented by arbitrarily setting to zero all terms with subscript $n > N$ in (2.11) and (2.12) and this defines a truncation of order N.

Substitution of (2.8) and (2.11) in (2.5) leads to:

For $t \geqslant 0$,

$$f_n(0, t) = \frac{\partial f_n}{\partial \xi}(0, t) = 0 \qquad \text{for} \quad n = 0, 1,...,$$
$$g_n(0, t) = \frac{\partial g_n}{\partial \xi}(0, t) = 0 \qquad \text{for} \quad n = 1, 2,..., \quad (2.18)$$

and

$$g_n(\xi, t) = 0 \qquad \text{for} \quad n = 1, 2,...,$$
$$f_k(\xi, t) = 0 \qquad \text{for} \quad k = 2, 3,..., \quad (2.19)$$
$$f_0(\xi, t) = \omega\xi \qquad \text{and} \qquad f_1(\xi, t) = -(e^{\xi} - e^{-\xi}) \text{ as } \xi \to \infty.$$

Two advantages of solving the original problem in this fashion as opposed to a numerical integration of the original partial differential equations are as follows: For a given Reynolds number the computer time necessary to generate a solution in terms of the Fourier series expansion is less than that required to integrate the original partial differential equation. Secondly, it is possible to use a small grid size h with a reasonably large field length ξ_∞ without encountering the computer core limitations when methods based on two-dimensional finite differences are used.

3. Numerical Solution Technique

Equations (2.13), (2.14), (2.15) and (2.16) along with boundary conditions (2.18) and (2.19) form a coupled nonlinear infinite system of differential equations to be solved for f_0, f_n, g_n, F_0, F_n and G_n. Once this system is solved, the flow field is

known since the stream and vorticity functions can be reconstructed from the assumed convergent series expansions (2.11) and (2.12). The infinite system given by (2.13), (2.14), (2.15) and (2.16) is made finite by truncating the stream and vorticity functions series (2.11) and (2.12) at N. That is, we set

$$f_n(\xi) = F_n(\xi) = g_n(\xi) = G_n(\xi) = 0 \qquad \text{for} \quad n > N. \tag{3.1}$$

For computation, the mesh constant $h = \Delta\xi = \pi/40$ was selected, and the infinity boundary conditions were imposed at large distance $r_\infty = e^{59\pi/40} = 102.909$. Selected values of Δt and $\Delta\xi$ satisfy the linear theory stability condition $\Delta t/(\Delta\xi)^2 \leqslant e^{2(k-1)h}\,\mathrm{Re}/4$. The system of equations (2.13), (2.14), (2.15) and (2.16) was integrated numerically by the following steps:

(1) At time $t = 0$, we selected zero for all values of f_0, f_n, g_n, F_0, F_n and G_n for $n = 1, 2,..., N$ except f_1 where we take $f_1 = -(e^{\xi} - e^{-\xi})$.

(2) The system of (2.13) along with boundary conditions

$$f_0(0, t) = f_n(0, t) = g_n(0, t) = 0 \qquad \text{for} \quad n = 1, 2,..., N$$

and

$$\begin{aligned} f_0(\xi_\infty, t) &= \omega\xi_\infty, \qquad f_1(\xi_\infty, t) = -(e^{\xi_\infty} - e^{-\xi_\infty}), \\ f_k(\xi_\infty, t) &= 0 \qquad \text{for} \quad k = 2, 3,..., N, \\ g_n(\xi_\infty, t) &= 0 \qquad \text{for} \quad n = 1, 2,..., N \end{aligned} \tag{3.2}$$

form the system of two-point boundary problems for f_0, f_n and g_n. The left-hand sides of (2.13) contain F_0, F_n and G_n whose values at all points in the field of computation are known at each time step. Central differences are used to approximate the space derivatives in (2.13), which give the approximation

$$f_n(\xi, t) = \frac{f_n(\xi + h, t) - h^2 e^{2\xi} F_n(\xi, t) + f_n(\xi - h, t)}{2 + n^2h^2} \qquad \text{for} \quad n = 0, 1,..., N$$

and

$$g_n(\xi, t) = \frac{g_n(\xi + h, t) - h^2 e^{2\xi} G_n(\xi, t) + g_n(\xi - h, t)}{2 + n^2h^2} \qquad \text{for} \quad n = 1, 2,..., N. \tag{3.3}$$

Equations (3.3) along with (3.2) are solved by iterations until a sufficient convergence 10^{-5} is obtained at all interior grid points for the values of f_0, f_n and g_n. Also, Eqs. (3.3) along with (3.2) can be solved explicitly for the unknowns, thereby eliminating any iterative operations.

(3) The values of F_0, F_n and G_n on the surface of the cylinder can be explicitly obtained from the boundary conditions (2.18).

Substituting the values of $f_0(0, t), f_n(0, t)$ and $g_n(0, t)$ from (2.18) in (2.13) and then approximating the second derivatives by central differences, one gets:

For $t \geqslant 0$

$$F_n(0, t) = \frac{f_n(-1, t) - 2f_n(0, t) + f_n(1, t)}{h^2} \quad \text{for} \quad n = 0, 1,..., N$$

and (3.4)

$$G_n(0, t) = \frac{g_n(-1, t) - 2g_n(0, t) + g_n(1, t)}{h^2} \quad \text{for} \quad n = 1, 2,..., N,$$

where $-1, 0, 1$ are the points shown in Fig. 2.

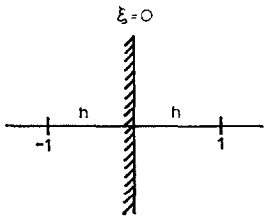

FIGURE 2.

Approximating the first derivatives of f_0, f_n and g_n in (2.18) by central differences, one gets:

For $t \geqslant 0$,

$$f_n(-1, t) = f_n(1, t) \quad \text{for} \quad n = 0, 1,..., N$$

and (3.5)

$$g_n(-1, t) = g_n(1, t) \quad \text{for} \quad n = 1, 2,..., N.$$

Substitution of (3.4) and $f_n(0, t)$ and $g_n(0, t)$ from (2.18) in (3.3) gives:

For $t \geqslant 0$,

$$F_n(0, t) = \frac{2f_n(1, t)}{h^2} \quad \text{for} \quad n = 0, 1,..., N$$

and (3.6)

$$G_n(0, t) = \frac{2g_n(1, t)}{h^2} \quad \text{for} \quad n = 1, 2,..., N.$$

Knowing f_0, f_n and g_n, the values of F_0, F_n and G_n were calculated on the surface of the cylinder using (3.6) with corresponding n.

(4) Time was increased by Δt; i.e., $t_{\text{new}} = t_{\text{old}} + \Delta t$.

(5) Substituting central differences for the space derivatives and forward differences for the time derivative in (2.14), one gets

$$F_0(\xi, t + \Delta t) = F_0(\xi, t) + \Delta t\, e^{-2\xi}\left[\frac{2(F_0(\xi + h, t) - 2F_0(\xi, t) + F_0(\xi - h, t))}{\mathrm{Re}\, h^2}\right.$$

$$+ \sum_{m=1}^{N} \frac{m}{4h}(-f_m(\xi, t)(G_m(\xi + h, t) - G_m(\xi - h, t))$$

$$+ g_m(\xi, t)(F_m(\xi + h, t) - F_m(\xi - h, t))$$

$$+ F_m(\xi, t)(g_m(\xi + h, t) - g_m(\xi - h, t))$$

$$\left. - G_m(\xi, t)(f_m(\xi + h, t) - f_m(\xi - h, t))\right]. \tag{3.7}$$

Similar finite-difference equations for F_n and G_n can be obtained from (2.15) and (2.16).

As $r \to \infty$, $\xi \to \infty$ and $\zeta = 0$ as $r \to \infty$; therefore, (2.12) gives:

For $t \geqslant 0$,

$$F_n(\xi_\infty, t) = 0 \qquad \text{for} \quad n = 0, 1, \ldots, N$$

and (3.8)

$$G_n(\xi_\infty, t) = 0 \qquad \text{for} \quad n = 1, 2, \ldots, N.$$

The values of F_0, F_n and G_n were calculated at a new time t by using the finite difference equations of F_0, F_n and G_n along with (2.17) and (3.8).

(6) Step (2) was repeated.

(7) Step (3) was repeated.

All of these steps were repeated at further times.

The force acting on the cylinder surface arises from the surface pressure and shear forces. In terms of nondimensional local surface pressure and tangential shear forces, the drag coefficient C_D and the lift coefficient C_L are given by

$$C_D = \int_0^{2\pi} (p \cos\theta + \sigma_{\xi\theta} \sin\theta)\Big|_{\xi=0} d\theta, \tag{3.9}$$

$$C_L = \int_0^{2\pi} (-p \sin\theta + \sigma_{\xi\theta} \cos\theta)\Big|_{\xi=0} d\theta, \tag{3.10}$$

where

$$\sigma_{\xi\theta} = \frac{4e^{-\xi}}{\mathrm{Re}}\left(\frac{\partial u}{\partial\theta} + \frac{\partial v}{\partial\xi} - v\right). \tag{3.11}$$

Substituting the values of u and v in terms of ψ in (3.11) and then substituting $\sigma_{\xi\theta}$ and $p(0, \theta, t)$ in (3.9) and (3.10) and using (2.11), one obtains after integration

$$C_D = \frac{4\pi}{\mathrm{Re}} \left(\frac{\partial^3 f_1}{\partial \xi^3} - 3 \frac{\partial^2 f_1}{\partial \xi^2}\right)\Big|_{\xi=0}, \tag{3.12}$$

$$C_L = \frac{4\pi}{\mathrm{Re}} \left[2 \left(\frac{\partial^3 f_0}{\partial \xi^3} - 2 \frac{\partial^2 f_0}{\partial \xi^2}\right) - \left(\frac{\partial^3 g_1}{\partial \xi^3} - 2 \frac{\partial^2 g_1}{\partial \xi^2}\right)\right]\Big|_{\xi=0}. \tag{3.13}$$

Using (2.13), (3.12) and (3.13) can be reduced to

$$C_D = \frac{4\pi}{\mathrm{Re}} \left(\frac{\partial F_1}{\partial \xi} - F_1\right)\Big|_{\xi=0}. \tag{3.14}$$

$$C_L = \frac{4\pi}{\mathrm{Re}} \left(-2 \frac{\partial F_0}{\partial \xi} + \frac{\partial G_1}{\partial \xi} - G_1\right)\Big|_{\xi=0}. \tag{3.15}$$

The pressure coefficient C_p on the surface of the cylinder is given by

$$C_p(\theta, t) = p(0, \theta, t) - p_\infty, \tag{3.16}$$

where p_∞ is the pressure at large distance ξ_∞ from the cylinder.

It may be shown that

$$\begin{aligned} C_p(\theta, t) = &- \frac{4}{\mathrm{Re}} \left\{\frac{\partial F_0}{\partial \xi} \theta + \sum_{n=1}^{N} \left[\frac{\partial F_n}{\partial \xi} \left(\frac{1 - \cos n\theta}{n}\right) + \frac{\partial G_n}{\partial \xi} \left(\frac{\sin n\theta}{n}\right)\right]\right\}\Big|_{\xi=0} \\ &+ 2 \int_0^{\xi_\infty} \left\{\left(\sum_{n=1}^{N} n \frac{\partial f_n}{\partial t}\right) - e^{-2\xi} \left[\left(\sum_{m=1}^{N} m^2 g_m\right)\left(\omega - \frac{\partial f_0}{\partial \xi} - \sum_{n=1}^{N} \frac{\partial g_n}{\partial \xi}\right)\right.\right. \\ &+ \left(\sum_{m=1}^{N} m f_m\right)\left(\sum_{n=1}^{N} n \left(f_n - \frac{\partial f_n}{\partial \xi}\right)\right) + \left(\frac{\partial f_0}{\partial \xi} - \omega + \sum_{n=1}^{N} \frac{\partial g_n}{\partial \xi}\right)^2 \\ &\left.\left. + \frac{2}{\mathrm{Re}} \sum_{n=1}^{N} n F_n\right]\right\} d\xi. \end{aligned} \tag{3.17}$$

The required integration in (3.17) were performed numerically using the calculated values at a given instant.

4. Results, Discussion, and Conclusion

The numerical calculations were done on a CDC 3150 at Humboldt State University, Arcata, California. A summary of parameters is given in Table I.

TABLE I

Re	Δt	$\Delta \xi$	N	r_∞	Final time	Approximate length of computer time (hr)
100	0.01	$\pi/40$	25	102.909	177.7	189
100	0.01	$\pi/40$	40	102.909	177.7	457
200	0.01	$\pi/40$	40	102.909	112.	293
500	0.01	$\pi/40$	40	102.909	77.	203

All the solutions presented were obtained by rotating the cylinder in the following way:

$$\begin{aligned} \omega &= 0, && 0 \leqslant t \leqslant 10, \\ &= 0.03, && 10 < t < 11, \\ &= 0, && t = 11, \\ &= -0.03, && 11 < t < 12, \\ &= 0, && t \geqslant 12. \end{aligned}$$

This is necessary since the calculations done without rotation for Re = 60 to 600 for a reasonably long time do not show a trace of asymmetric flow. The same rotation was used for all the Reynolds numbers in order to compare the effect of rotation on the Reynolds numbers.

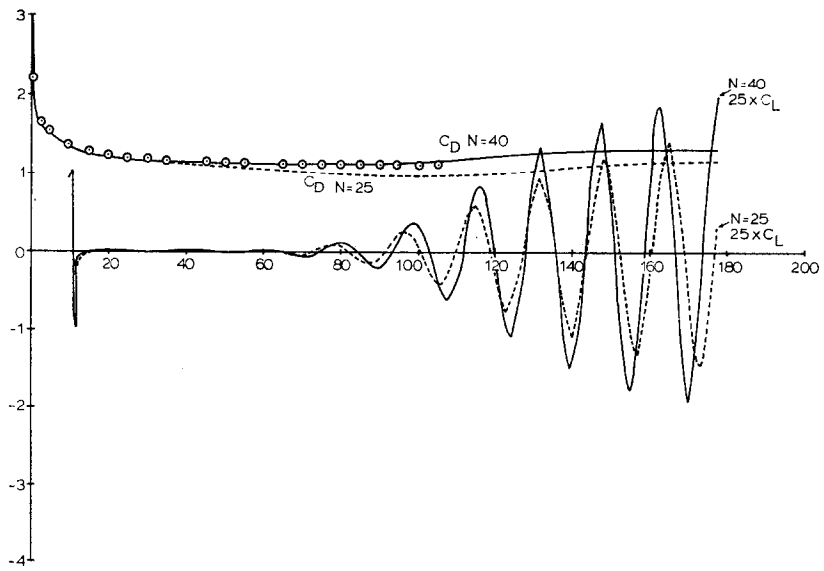

FIG. 3. The development of C_D and C_L with time at Re = 100: Comparison between calculated values of C_D : - - - $N = 25$; —— $N = 40$, this study; ○, Patel [21]; comparison between calculated values of C_L : - - - $N = 25$, —— $N = 40$, this study.

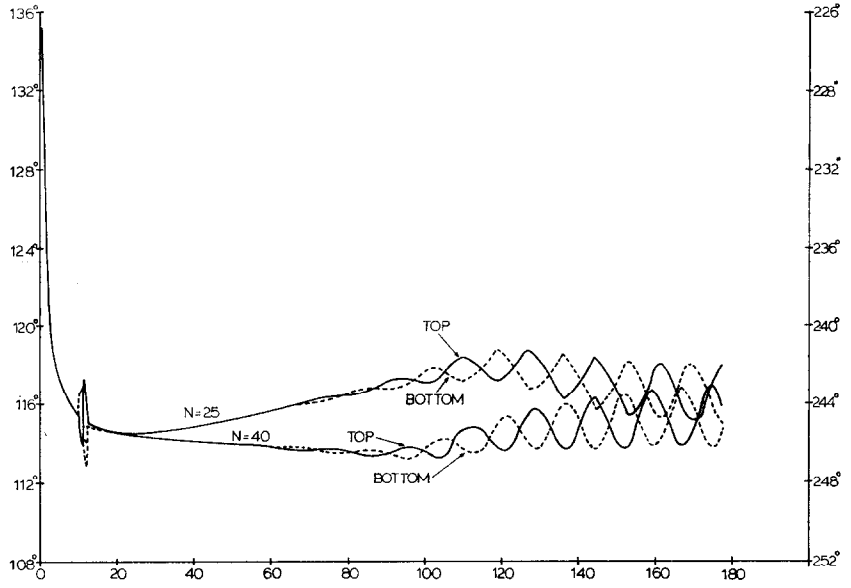

FIG. 4. The development of the separation angles with time at Re = 100 with different N.

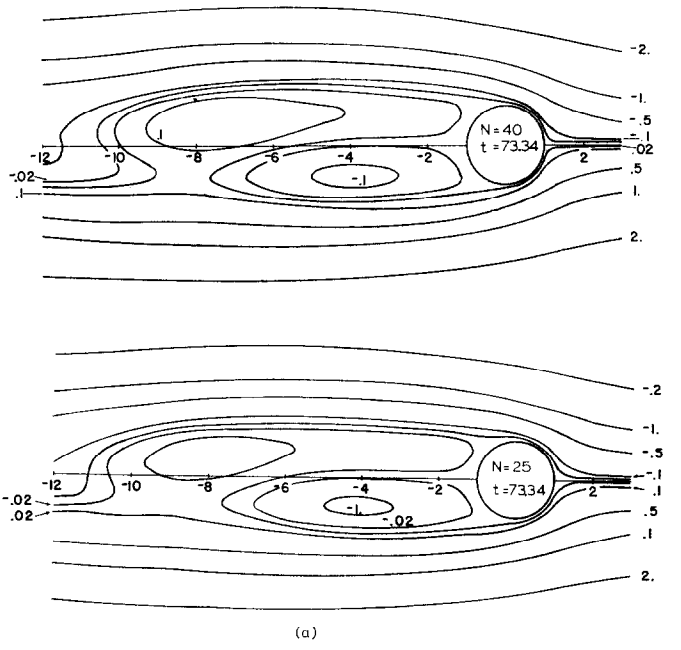

(a)

FIG. 5. The development of streamlines with time at Re = 100 with different N.

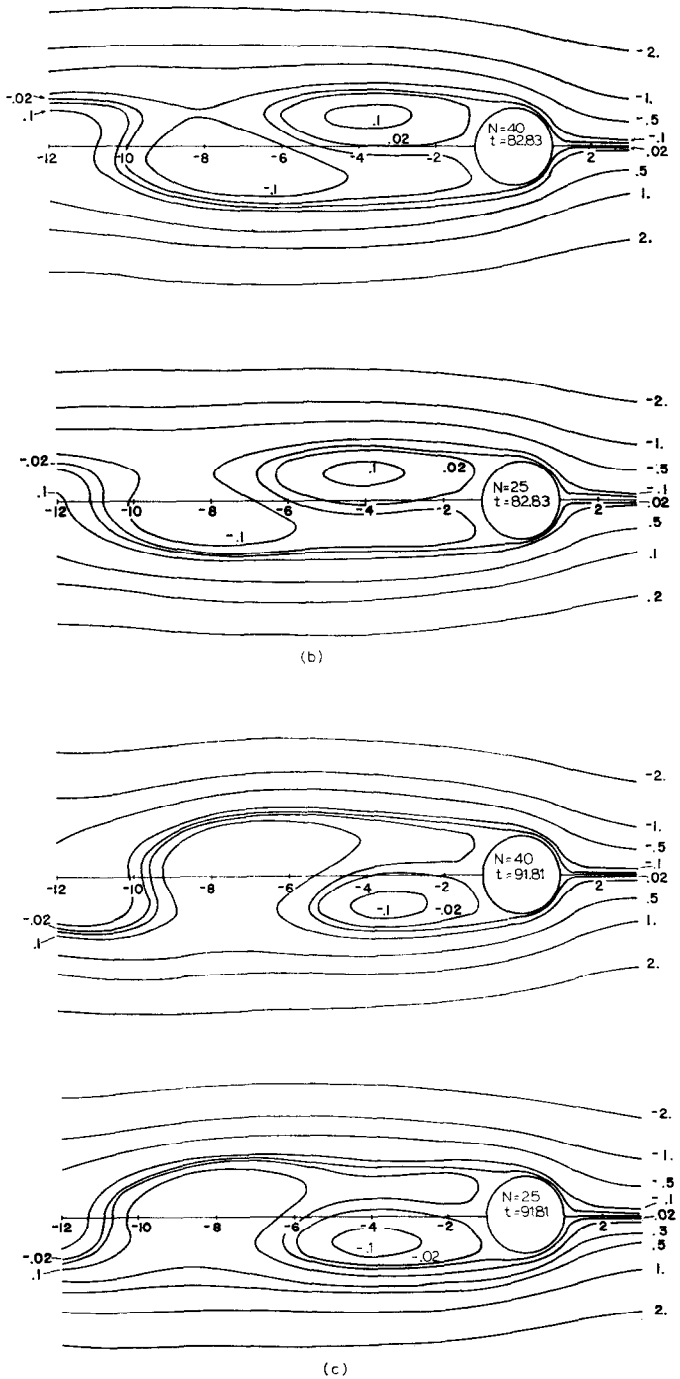

(b)

(c)

FIG. 5 — *Continued.*

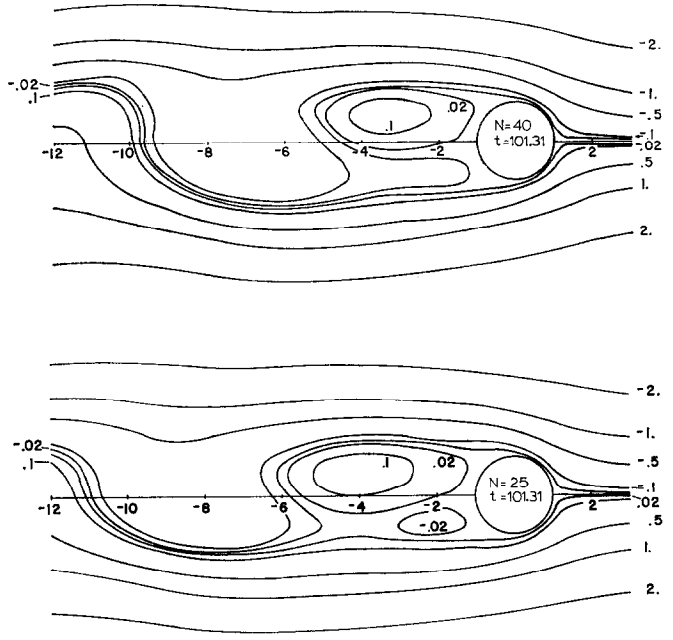

(d)

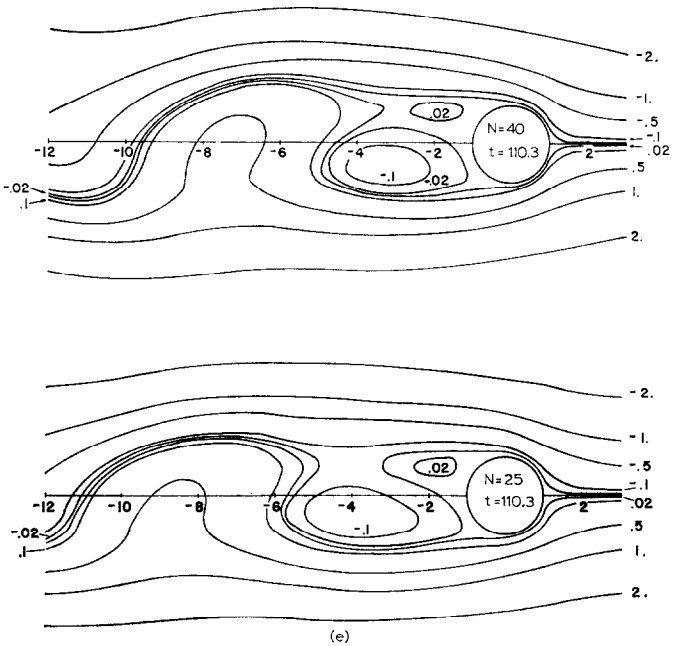

(e)

FIG. 5 — *Continued.*

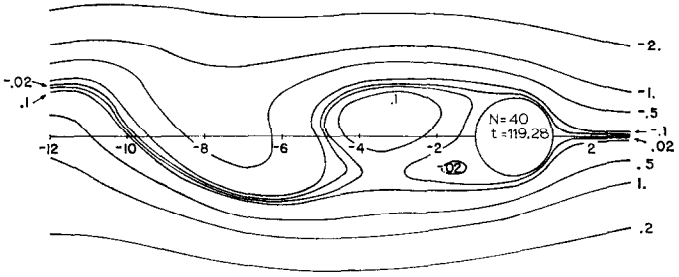

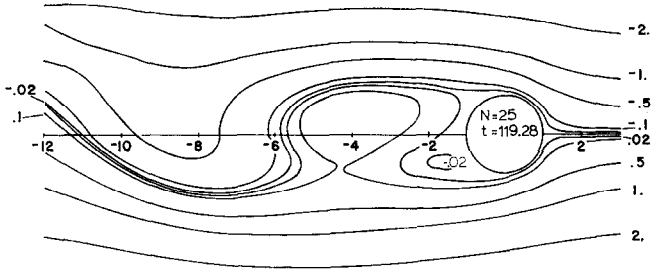

(f)

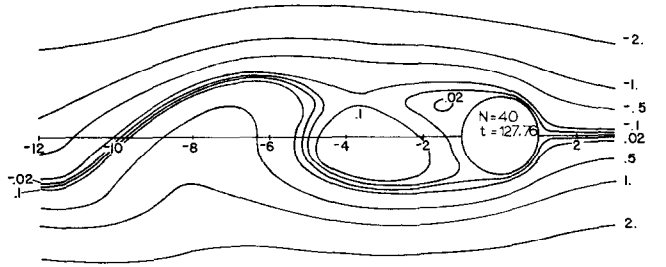

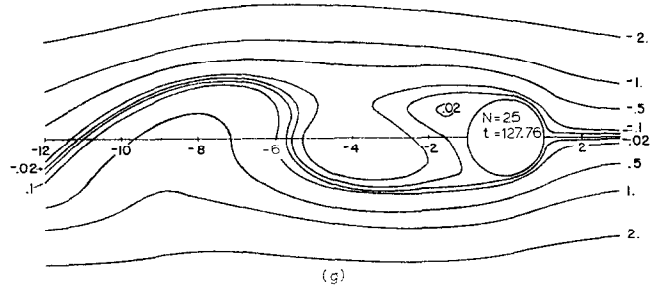

(g)

FIG. 5 — *Continued.*

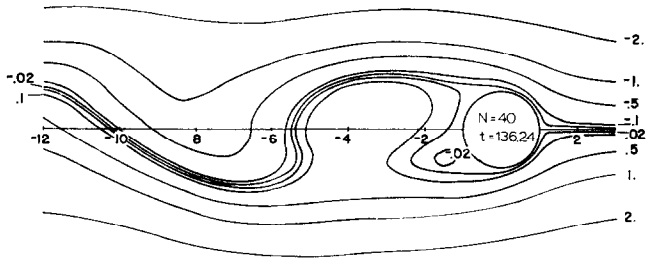

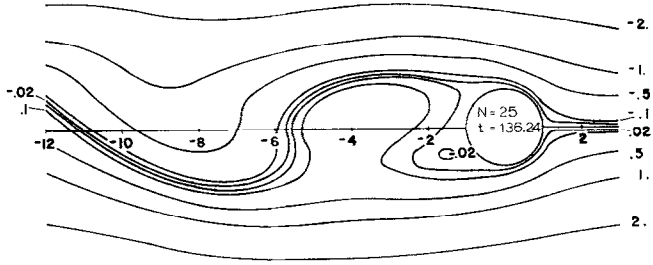

(h)

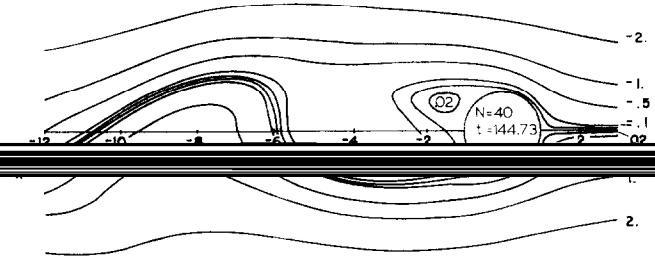

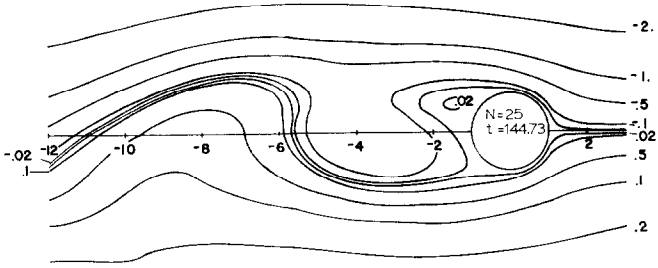

(i)

FIG. 5 — *Continued.*

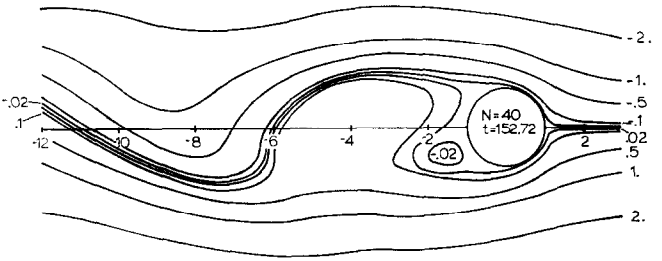

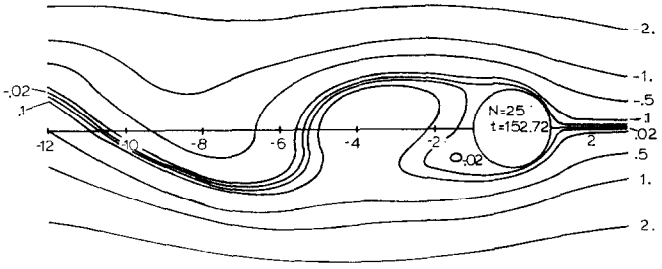

(j)

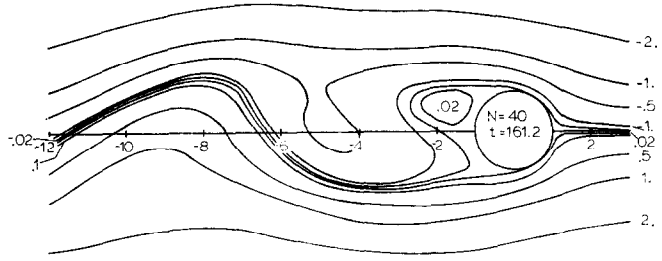

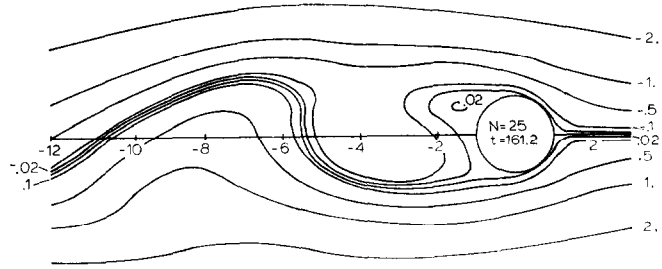

(k)

FIG. 5 — *Continued.*

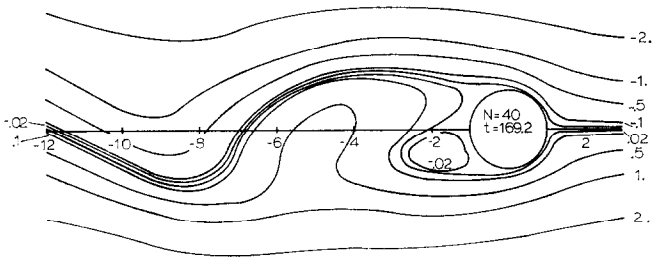

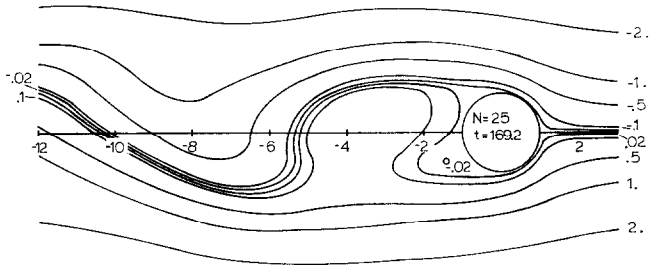

(l)

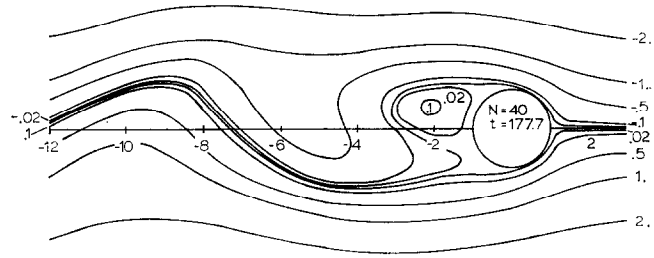

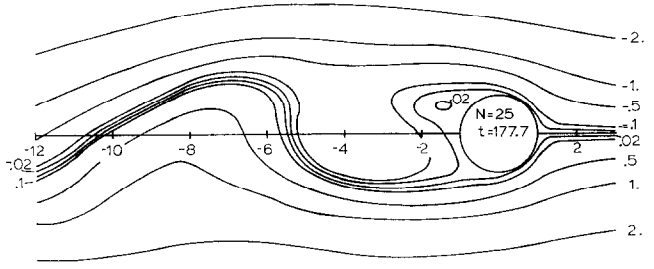

(m)

FIG. 5 — *Continued.*

Reynolds Number 100

For Re = 100, the development of the drag C_D and the lift C_L with time with $N = 25$ and $N = 40$ is shown in Fig. 3 along with the symmetrical calculations of drag of Patel [21] using $N = 60$. There is excellent agreement for C_D with $N = 40$ with the results obtained by Patel. The angle on the surface of the cylinder at which the vorticity changes its sign gives the separation angle. The vorticity on the surface of the cylinder was computed by using (2.12). The development of the separation angles is plotted as a function of time at Re = 100 with $N = 25$ and $N = 40$ in Fig. 4. The small rotation that is applied at early stage starts a sudden lift and a sudden change in separation of top and bottom angles. Once the rotation is removed, the lift drops in the vicinity of zero and the separation almost becomes symmetric. This small rotation has not left a long duration effect. After $t = 60$, the effect becomes clearly visible. The lift and the separation angles oscillate as a result of vortex shedding. The amplitude of the lift and the separation angles increase as time increases. Figure 5

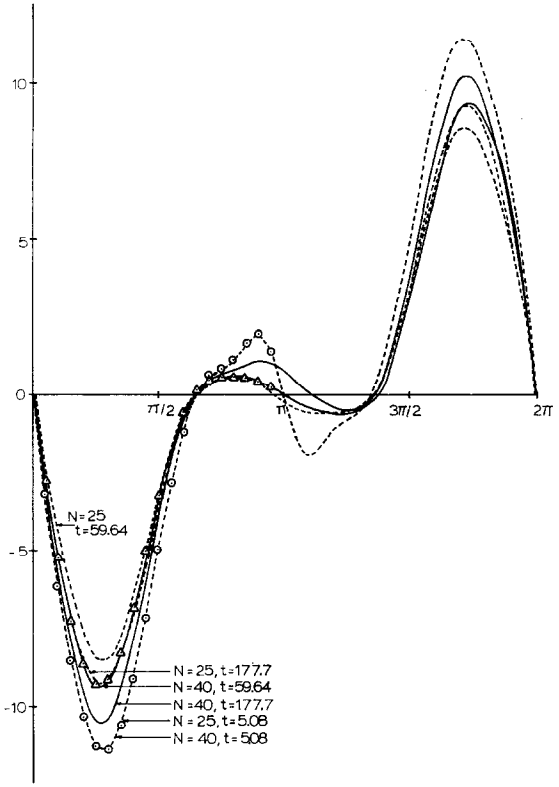

FIG. 6. The development of surface vorticity distribution with time at Re = 100 with different N: Comparison between calculated values of vorticity distribution: ○, Patel [21] at $t = 5.08$; △, Patel [21] at $t = 59.64$; – – –, $N = 25$, —— $N = 40$, this study.

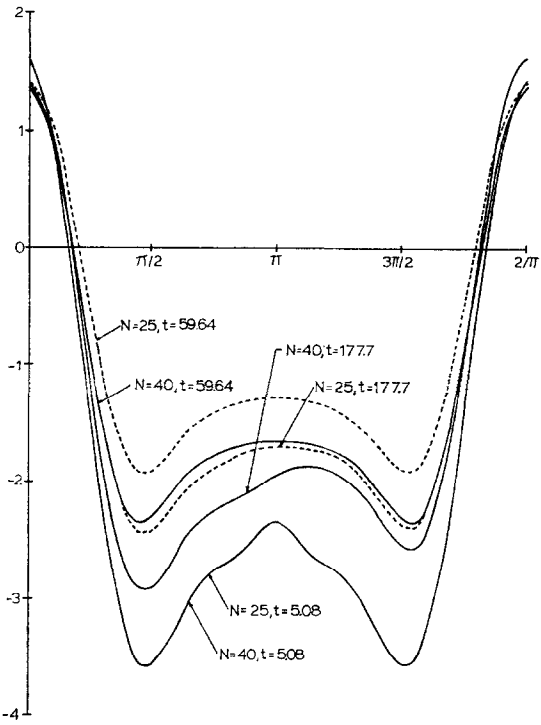

FIG. 7. The development of surface pressure distribution with time at Re = 100 with different N.

shows the development of streamlines with $N = 40$ and $N = 25$ at Re = 100. At early stage the vortex pair grows symmetrically. Initially, the effect of rotation is hardly detectable; however, as time progresses the rotation causes the vortices to oscillate relative to each other as can be seen in Figs. 5a, b, and c. This oscillation is is very small at first but increases with time. Eventually, one of the vortices is captured by the stream of flow from the opposite side of the cylinder. This marks the beginning of the vortex shedding and the vortices continue to be shed alternately from the two sides of the cylinder. More terms help to form and stretch the vortices, as can be seen by comparing the streamlines at a given instant with $N = 40$ and $N = 25$ in Fig. 5. The flow pattern in Fig. 5 illustrates the pattern when the lift is in the vicinity of zero for $N = 25$. There are no strong vortices near the cylinder in such cases. However in Fig. 5m for $N = 40$, there is a strong vortex behind the cylinder. Note that in this case the lift is maximum. When the lift is maximum or minimum, the separation points of the top and the bottom are symmetric. The lift and separation points oscillate at one-half of Strouhal frequency. The Strouhal number evaluated from the last cycle of a lift curve has a value 0.125 for $N = 25$ and 0.133 for $N = 40$. Figure 6 shows the development of vorticity distribution around the surface of the cylinder with $N = 40$ and $N = 25$ along with the similar symmetrical calculations with $N = 60$ of Patel [21]. There is excellent agreement between the vorticity cal-

culations with $N = 40$ and $N = 25$ at $t = 5.08$. Figure 7 shows the development of surface pressure distribution with $N = 40$ and $N = 25$ at Re $= 100$. Excellent agreement can be seen between surface pressure calculations with $N = 25$ and $N = 40$ initially. A developed kink can be seen at $t = 5.08$ in Fig. 6 and Fig. 7. There is excellent agreement between the calculations of surface vorticity at $t = 5.08$ with $N = 40$ and the symmetrical calculations of Patel with $N = 60$. Also, there is very good agreement between the calculations of surface voricity at $t = 59.64$ for $N = 40$ and the symmetrical calculations of Patel for $N = 60$ even though the cylinder was rotated in the case of $N = 40$ for a short time. There is a significant difference between the surface vorticity and surface pressure calculations at $t = 59.64$ and 177.7 with $N = 25$ and 40. This is due to the number of terms and the length of time interval.

Reynolds Number 200

For Re $= 200$, Fig. 8 shows the development of C_D and C_L with time. Also in Fig. 8, the development of C_D is compared with the results obtained by Patel using

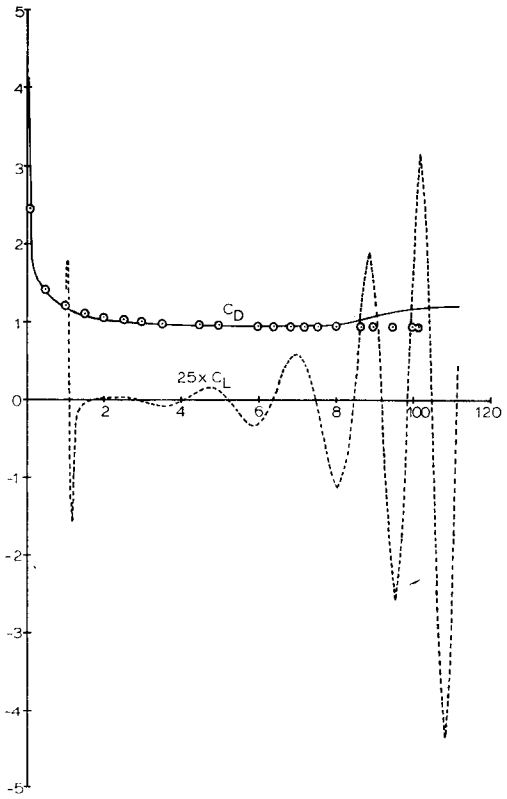

FIG. 8. The development of C_D and C_L with time at Re $= 200$: Comparison between calculated values of C_D : ——, this study; ⊙, Patel [21]; calculated values of C_L : – – –, this study.

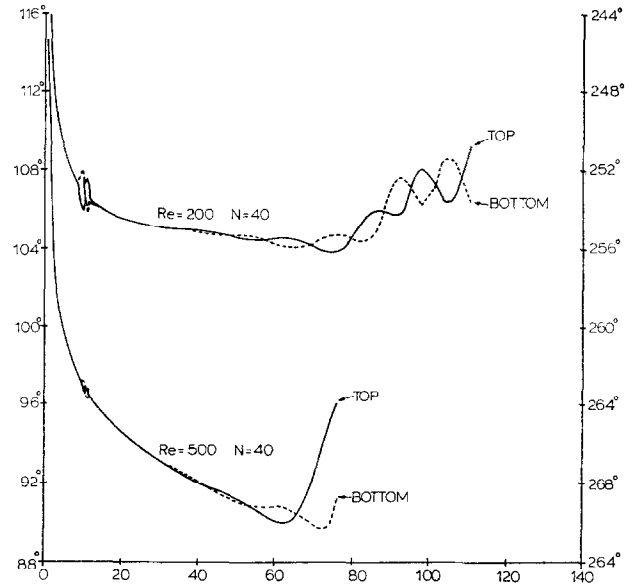

Fig. 9. The development of the separation angles with time at Re = 200 and 500.

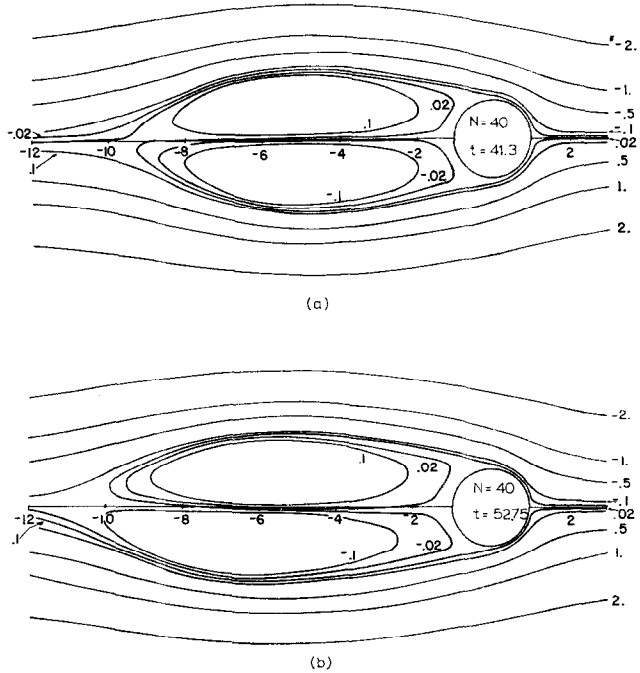

FIG. 10. The development of streamlines with time at Re = 200.

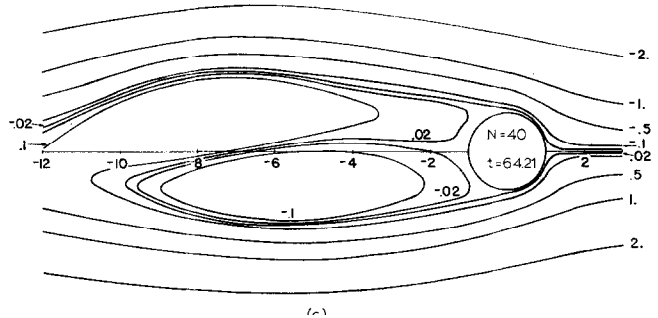

(c)

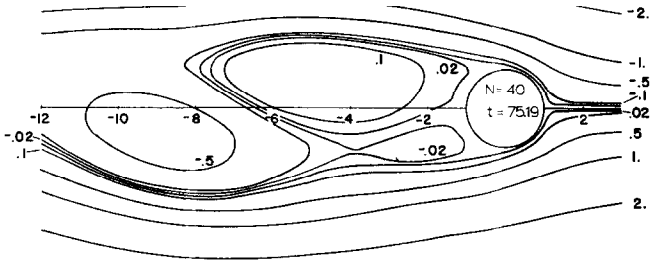

(d)

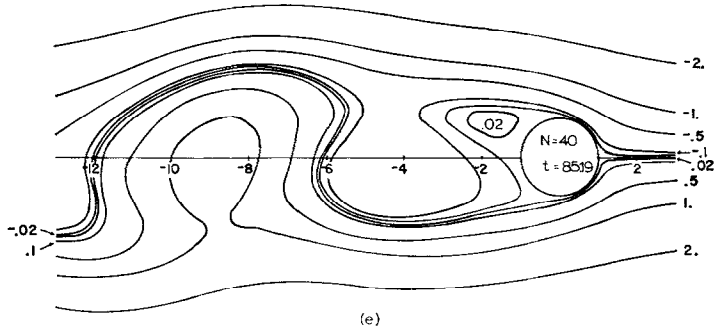

(e)

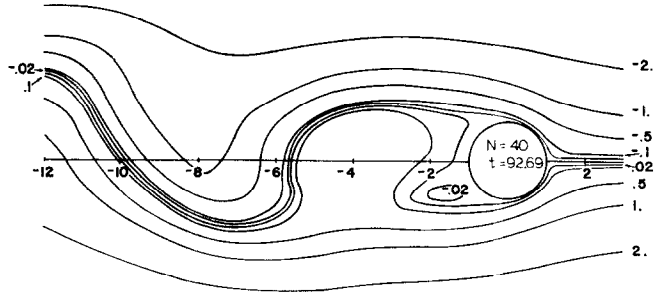

(f)

FIG. 10 — *Continued.*

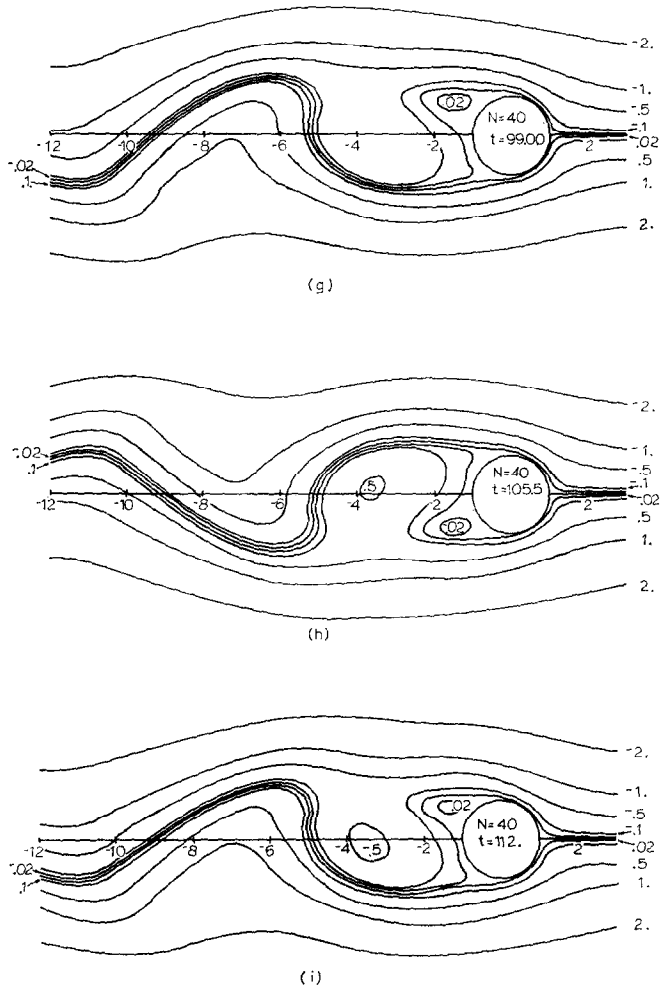

FIG. 10 — *Continued.*

$N = 60$. The results are in very good agreement up to $t = 80$. The development of separation angles is plotted as a function of time using $N = 40$ in Fig. 9. After $t = 30$, the effect of small rotation becomes clearly visible. Figure 10 shows the development of the flow pattern with time. The Strouhl numbers evaluated from the cyclic lift curves are compared with experimental results and similar calculations in Table II. The development of surface vorticity distribution along with the similar symmetrical calculations of Patel [21] is shown in Fig. 11. There is excellent agreement with the symmetrical calculations of Patel at $t = 15.16$ and $t = 45.02$. The development of surface pressure distribution at Re $= 200$ is shown in Fig. 12. In Figs. 11 and 12, a developed kink can be seen at $t = 15.16$.

TABLE II
Comparison of Strouhal Number

Re	Strouhal number	Author(s)
100	0.16	Roshko [7]
	0.16	Jordan and Fromm [12]
	0.119 (Average)	$N = 25$ (present)
	0.125 (Last cycle)	
	0.128 (Average)	$N = 40$ (present)
	0.133 (Last cycle)	
200	0.10	Dawson and Marcus [13]
	0.15	Thoman and Szewczyk [11]
	0.17	Jain and Goel [14]
	0.18	Lin, Pepper, and Lee [15]
	0.16	Relf and Simmons [6]
	0.17–0.19	Roshko [7]
	0.136 (Average)	$N = 40$ (present)
	0.154 (Last cycle)	

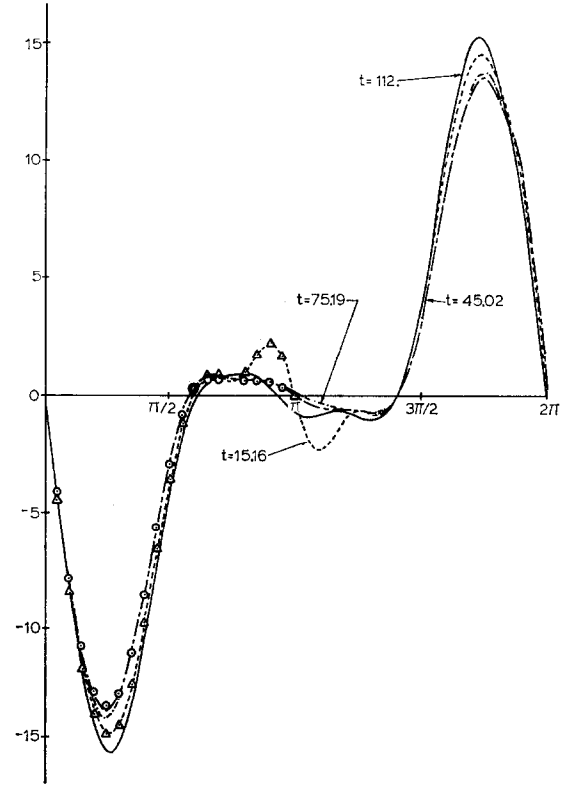

FIG. 11. The development of surface vorticity distribution with time at Re = 200: Comparison between calculated values of vorticity distribution: △, Patel [21] at $t = 15.16$; ○, Patel [21] at $t = 45.02$; – – – at $t = 15.16$, — — — at $t = 45.02$, — · — · at $t = 75.19$, —— at $t = 112$, this study.

Reynolds Number 500

Figure 13 shows the development of C_D and C_L with time for Re = 500 with $N = 40$ along with the symmetrical calculations of C_D of Patel using $N = 60$. Figure 9 shows the development of separation angles with time. The development of the flow pattern with time is shown in Fig. 14. The rotation causes the vortices to oscillate relative to each other. One of the vortices is captured by the stream of flow from the opposite

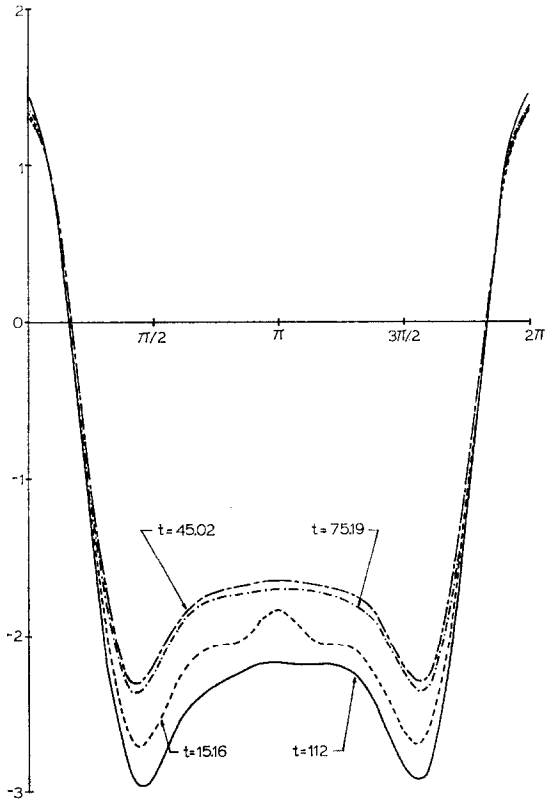

FIG. 12. The development of surface pressure distribution with time at Re = 200.

side of the cylinder. This marks the beginning of the vortex shedding. The number of iterations required for convergence and ever increasing lift forced us to conclude that the system breaks down. The oscillating vortex shedding was not observed and therefore the Strouhal number cannot be computed. The development of vorticity distribution is shown in Fig. 15 along with the similar calculations of Patel. The vorticity distribution at $t = 15.66$ clearly shows the secondary vortices in the wake as a region of opposite vorticity. The secondary vortices were observed earlier than $t = 3.97$ and disappeared completely at $t = 31.4$. The rotation clearly affects the

size of the secondary vortices. Also, the secondary vortices were observed earlier than $t = 4$ at Re $= 490$. The development of surface pressure distribution at Re $= 500$ is shown in Fig. 16.

The number of terms and the imposition of the free stream boundary condition at a finite distance play an important role in determining the separation points, lift, drag, Strouhal number, and flow patterns. The questions are: How many terms are enough ? What is the effect of imposing free stream boundary conditions at $r = 102.9$?

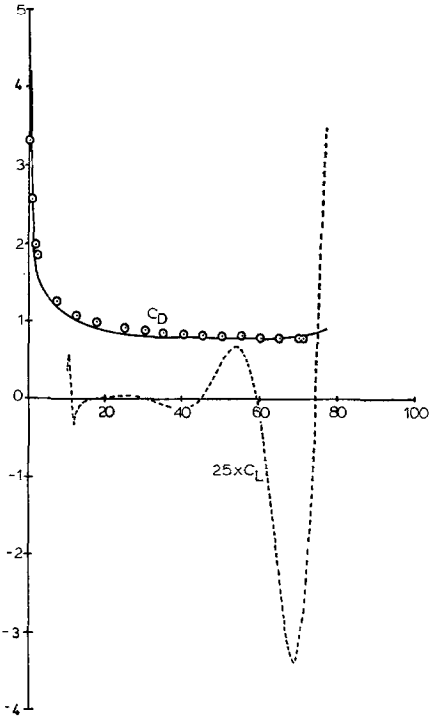

FIG. 13. The development of C_D and C_L with time at Re $= 500$: Comparison between calculated values of C_D : ——, this study; ○, Patel [21]; Calculated values of C_L : – – –, this study.

The calculated drag and vorticity surface distributions for $N = 40$ are in very good agreement with the symmetrical calculations of Patel [21] for $N = 60$ at Re $= 100$, 200 and 500. In the first case the free stream boundary conditions were imposed at $r = 102.9$ and in the second case at $r = 169.25$. Even at Re $= 490$ and 500, the calculations for $N = 40$ show the secondary vortices. It seems that the outer boundary ($r_\infty = 102.9$) is far away not to have any appreciable effect on the wake behind the cylinder. Therefore it is very reasonable to assume that the results presented with $N = 40$ are reasonably accurate.

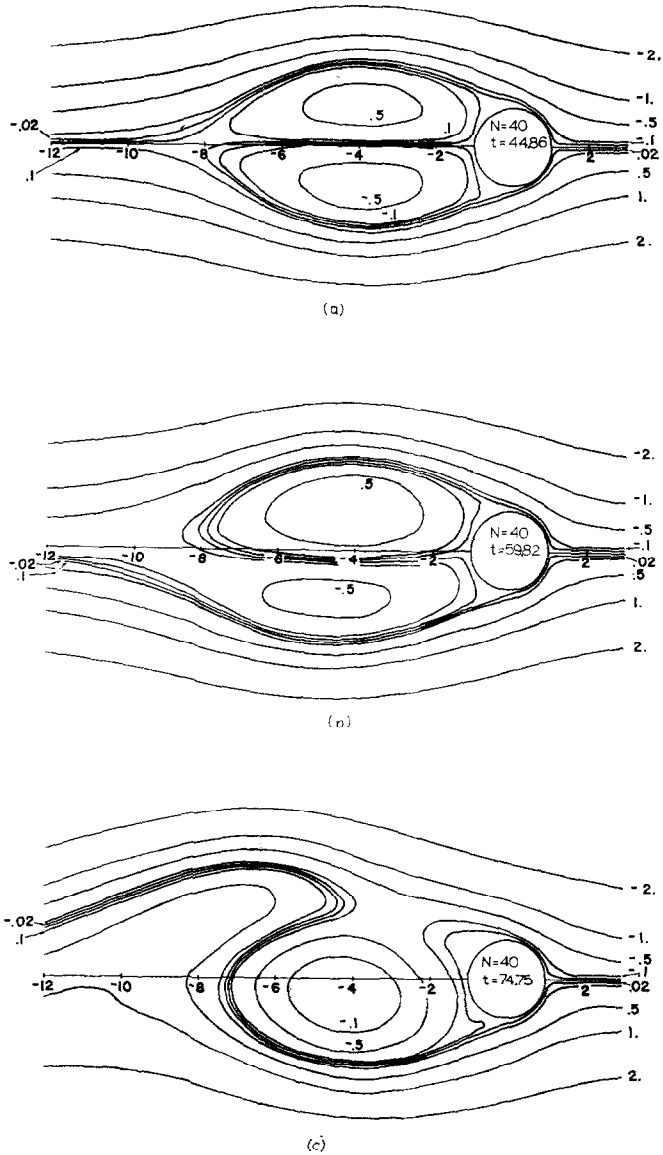

FIG. 14. The development of streamlines with time at Re = 500.

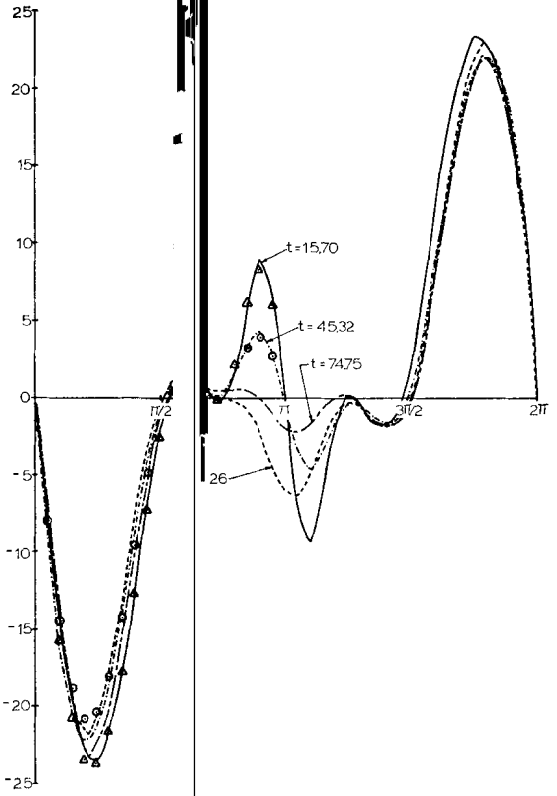

FIG. 15. The de ppment of surface vorticity distribution with time at R 500: Comparison between calculated values of vorticity ribution: △, Patel [21] at $t = 15.7$; ○, Patel [21] at t 45.32; —— at $t = 15.7$, — · — · at $t = 45.32$, - - - at t 9.26, — - — - at $t = 74.75$, this study.

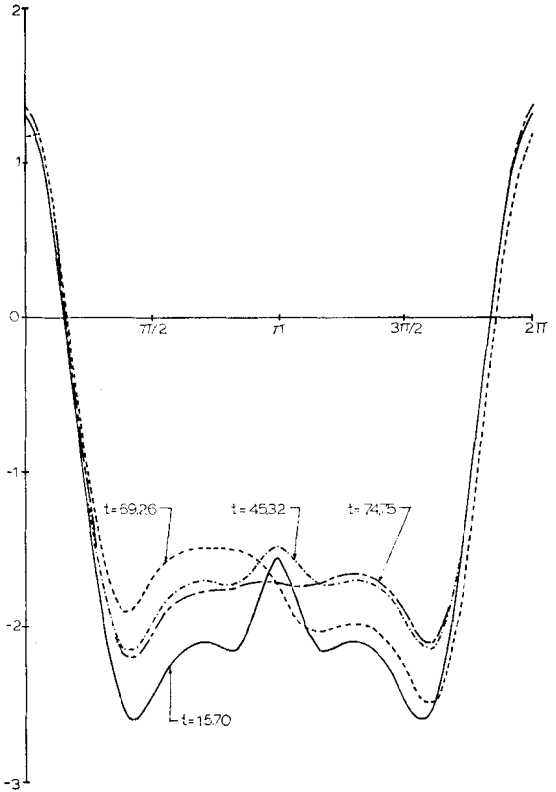

FIG. 16. The development of surface pressure distribution with time at Re = 500.

REFERENCES

1. F. HOMANN, *Forsch. Geb. Ing. Wes.* 7 (1936), 1.
2. L. S. G. KOVASZNAY, *Proc. Roy. Soc. A* **198** (1949), 174.
3. S. TANEDA, *J. Phys. Soc. Japan* **11** (1956), 302.
4. H. BÉNARD, *C. R. Acad. Sci. Ser. B* **147** (1908), 839.
5. TH. VON KÁRMÁN, *Gött. Nachr.* (1911), 509.
6. E. F. RELF AND L. F. G. SIMMONS, Aero. Res. Council, London, R. & M. No. 917 (1924).
7. A. ROSHKO, NACA Report 1191 (1954).
8. P. C. JAIN AND K. S. RAO, *Phys. Fluids Suppl. II* **12** (1969), II-57.
9. J. E. FROMM AND F. H. HARLOW, *Phys. Fluids* **6** (1963), 975.
10. I. HIROTA AND K. MIYAKODA, *J. Met. Soc. Japan, Ser. II* **43** (1965), 30.
11. D. C. THOMAN AND A. A. SZEWCZYK, *Phys. Fluids Suppl. II* **12** (1969), II-76.
12. S. K. JORDAN AND J. E. FROMM, *Phys. Fluids* **15** (1972), 371.
13. C. DAWSON AND M. MARCUS, *in* "Proceedings of the 1970 Heat Transfer and Fluid Mechanics Institute" (T. Sarpakaya, Ed.), p. 323, Stanford Univ. Press, Stanford, Calif., 1970.
14. P. C. JAIN AND B. S. GOEL, *Computers and Fluids* **4** (1976), 137.
15. C. L. LIN, D. W. PEPPER, AND S. C. LEE, *AIAA J.* **14** (1976), 900.
16. S. M. DESAI, Ph.D. Thesis, University of California, Berkeley, 1965.
17. R. L. UNDERWOOD, *J. Fluid Mech.* **37** (1969), 95.
18. S. C. R. DENNIS AND M. SHIMSHONI, Aero. Res. Counc., London, Current Paper No. 797 (1965).
19. F. NIEUWSTADT AND H. B. KELLER, *Computers and Fluids* **1** (1973), 59.
20. W. M. COLLINS AND S. C. R. DENNIS, *J. Fluid Mech.* **60** (1973), 105.
21. V. A. PATEL, *Computers and Fluids* **4** (1976), 13.